High-temperature structural phase transitions in neighborite; a high-resolution neutron powder diffraction investigation

Kevin S. Knight[a,b], G. David Price[c], John A. Stuart[c,d] and Ian G. Wood[c,*]

[a] *ISIS Facility, STFC Rutherford Appleton Laboratory, Harwell Oxford, Didcot, Oxon. OX11 0QX, UK*

[b] *Department of Earth Sciences, The Natural History Museum, Cromwell Road, London SW7 5BD, UK*

[c] *Department of Earth Sciences, University College London, Gower Street, London WC1E 6BT, UK*

[d] *Present address: 12, Coneygreave Close, Cheadle, Stoke-on-Trent ST10 1NN, UK*

[*] Corresponding author: Tel.: +44 (0)20 7679 2405; fax +44 (0)20 7679 2433.

E-mail address: ian.wood@ucl.ac.uk (I.G. Wood)

ABSTRACT

The nature of the apparently continuous structural phase transition at 1049 K in the perovskite-structured, $MgSiO_3$ isomorph, neighborite ($NaMgF_3$), from the orthorhombic (*Pbnm*) hettotype phase to the cubic ($Pm\bar{3}m$) aristotype structure, has been re-investigated using high resolution, time-of-flight neutron powder diffraction. Using data collected at 1 K intervals close to the nominal phase transition temperature, the temperature-dependence of the intensities of superlattice reflections at the M point ($\frac{2\pi}{a}\left[\frac{1}{2},\frac{1}{2},0\right]$) and the R point (

$\frac{2\pi}{a}\left[\frac{1}{2},\frac{1}{2},\frac{1}{2}\right]$) of the pseudocubic Brillouin zone indicate the existence of a new intermediate tetragonal phase in space group *P*4/*mbm*, with a narrow phase field extending from ~1046.5 K to ~1048.5 K, at ambient pressure. Group theoretical analysis shows that the structural transitions identified in this study, *Pbnm* – *P*4/*mbm*, and *P*4/*mbm* - $Pm\bar{3}m$, are permitted to be second order. The observation of the tetragonal phase resolves the longstanding issue of why the high temperature phase transition, previously identified as *Pbnm* – $Pm\bar{3}m$, and which would be expected to be first order under Landau theory, is in fact found to be continuous. Analysis of the pseudocubic shear strain shows it to vary with a critical exponent of 0.5 implying that the phase transition from *Pbnm* to *P*4/*mbm* is tricritical in character. The large librational modes that exist in the MgF_6 octahedron at high temperature, and the use of Gaussian probability density functions to describe atomic displacements, results in apparent bond shortening in the Mg – F distances, making mode amplitude determination an unreliable method for determination of the critical exponent from internal coordinates. Crystal structures are reported for the three phases of $NaMgF_3$ at 1033 K (*Pbnm*), 1047 K (*P*4/*mbm*), and 1049 K ($Pm\bar{3}m$).

Keywords: Neighborite; $NaMgF_3$; Phase transitions; Neutron diffraction; $MgSiO_3$ perovskite; $MgSiO_3$ post-perovskite

Introduction

Knowledge of the physical properties of the perovskite and post-perovskite phases of $MgSiO_3$ is crucial to our understanding of the Earth's lower mantle. In particular, the D″ region on the mantle side of the core-mantle-boundary, which forms the mantle's lower thermal boundary layer, is associated with the transition in $MgSiO_3$ from the perovskite to post-perovskite

44 structure. For $MgSiO_3$, however, many of these properties are difficult to measure accurately
45 in the perovskite phase and most of them cannot be measured at the extreme pressures of
46 stabilisation of post-perovskite (120 GPa). The best chance of constraining them is through a
47 combination of measurements on low-pressure analogue materials (with the same crystal
48 structure but a different chemical composition) and *ab initio* simulations of both the analogue
49 and natural systems. Experimentally, fluoride analogue phases can be considered to have
50 advantages over oxides as their high-pressure phases become stable at much lower pressures.
51 Thus, for example, ABF_3 perovskites have been used in investigations of the viscosity and
52 electrical conductivity of the mantle (Poirier *et al.*, 1983; Watson *et al.*, 1995; Li and
53 Weidner, 2012). The seismic velocity changes in the D″ region have been interpreted via
54 measurements of the equations of state of perovskite and post-perovskite $NaMgF_3$ (Hustoft *et*
55 *al.*, 2008) and very recently, studies of the perovskite to post-perovskite transition in single
56 crystals of $NaNiF_3$ have greatly improved understanding of the possible development of
57 texture and the resulting seismic anisotropy in D″ (Dobson *et al.*, 2011; Dobson *et al.*, 2013).
58 The relatively low transition pressures found in the ABF_3 compounds also imply that their
59 ultrahigh pressure polymorphs, of relevance to super-Earths, might be investigated
60 experimentally as well as by computer simulations (Umemoto and Wentzcovitch, 2006;
61 Grocholski *et al.*, 2010).

62 $NaMgF_3$, found naturally as the mineral neighborite (Chao *et al.*, 1961), provides arguably
63 the closest fluoride analogue to $MgSiO_3$ as the two compounds are isoelectronic, have similar
64 ionic masses, and crystallise in both the orthorhombic (*Pbnm*) perovskite and post-perovskite
65 structures (see e.g. Umemoto *et al.*, 2006). Preliminary high-temperature crystallographic
66 investigations by Chao *et al.* (1961) indicated that neighborite undergoes at least one
67 structural phase transition at a temperature of ~1173(25) K. A tetragonal, or pseudotetragonal
68 phase was inferred to exist between 1033 K and 1173 K, however characterisation of this

phase was hampered by the limited real space resolution of the diffractometer employed. More recently, Zhao *et al.* (1993a,b) re-investigated the structural behaviour of neighborite at high temperature using higher-resolution synchrotron powder diffraction; they found no evidence for an intermediate phase, and a continuous transition to the aristotype cubic phase. This result is surprising as the *Pbnm* – $Pm\bar{3}m$ transition would be expected to be first order under conventional Landau theory (Tolédano and Tolédano , 1987), rather than continuous (unless, by accident, the critical temperatures of the two phonon modes of different symmetry are exactly, or very close to, the same temperature). Critical behaviour was inferred from an analysis of the magnitudes of the two independent order parameters (the in-phase, and anti-phase octahedral tilts; Glazer, 1972, 1975) with the conclusion that both modes condensed simultaneously with an identical critical exponent of 0.25, i.e. continuous tricritical behaviour in both order parameters. The crystallographic analysis performed, and the conclusions drawn from this study will be critiqued in detail in the Results and Discussion section of this communication.

The precise characterisation of the crystal structures of polycrystalline, zone-boundary tilted, perovskite-structured materials requires the ability both to determine the metric of the pseudocubic subcell of the hettotype phase and also to observe key diagnostic superlattice reflections at special points on the surface of the pseudocubic Brillouin zone (R, M, and X points; Glazer, 1975). For the former, data must be collected at the highest possible real space resolution, whereas for the latter, as the diagnostic superlattice reflections arise principally from the displacements of the anions, neutron powder diffraction offers significant advantages over X-ray diffraction, especially when the octahedral and the quasi-dodecahedral sites contain heavy metal cations and the anion species are light. We present here a re-investigation of the high-temperature phase transitions in the perovskite form of $NaMgF_3$. In this study, we have exploited the intrinsic advantages of neutron diffraction, using a powder

diffractometer with a high real space resolution ($\Delta d/d = 4 \times 10^{-4}$), which, to first order, is independent of the magnitude of the scattering vector.

Experimental

The powder sample for neutron diffraction was synthesised by solid state reaction of a stoichiometric mixture of NaF and MgF_2 (nominal purity 99.99%) at 750°C, for 15 h, in air (Street *et al.*, 1997). The ground and sieved powder was placed in an 11 mm diameter, cylindrical vanadium sample can and located in a vacuum furnace equipped with vanadium heat shields and element. Time-of-flight neutron powder diffraction data were collected in the range 30 – 130 ms, using the high resolution backscattering detectors of the powder diffractometer HRPD, at the ISIS spallation neutron source (Ibberson et al., 1992). Data were collected at the following temperatures: at 823 K, then in 10 K steps to 993 K, at 999 K, then in 10 K steps to 1029 K, in 2 K intervals to 1041 K, at 1044 K, then in 1 K steps to 1054 K. All data collections were made for 30 μAh (approximately 50 minutes) with a 10 minute thermal equilibration time once the set point temperature was achieved. Above 1054 K, data were collected in 5 K intervals to 1224 K, for 6 μAh, with a 10 minute equilibration time. Thermal stability was ±0.1 K for all temperatures.

The raw data were focussed, normalised to the incident flux distribution using an upstream beam monitor, and corrected for wavelength-dependent detector efficiency to produce a dataset in the time-of-flight range 32 – 120 ms, equivalent to 0.64 – 2.4 Å in the backscattering bank (maximum Q resolution 9.82 $Å^{-1}$), and suitable for profile refinement using the GSAS suite of programs (Larson and Von Dreele, 1986). Instrumental calibrations were made using SRM640b standard silicon powder to determine the time-of-flight (ms) to *d*-spacing (Å) conversion, and a ceramic CeO_2 pellet to characterise the intrinsic line shape

from the methane moderator. Data were analysed using the Rietveld method, as implemented within GSAS, using a pseudo-Voigt convoluted with back-to-back exponentials for the line shape. An initial model for the 999 K refinement was derived from the results of Zhao *et al.* (1993a); once this refinement had converged, the result was used as a seed for the next temperature, with the whole process carried out iteratively to the highest temperature measured. Atomic displacement parameters were refined as isotropic for both cations, and as anisotropic for the anions.

Discussion of earlier high-temperature crystallographic results

The structural behaviour of $NaMgF_3$ has been investigated by X-ray diffraction as a function of composition, with substitution of K for Na (Martin *et al.*, 2005), as a function of pressure at room temperature (Liu *et al.*, 2005; Martin *et al.*, 2006a,b), and at simultaneous high pressure and temperature (Chen *et al.*, 2005). At atmospheric pressure, X-ray diffraction at high temperature has been used to study both the orthorhombic and cubic phases, refining both the average (Zhao *et al.*, 1993a; Zhao *et al.*, 1993b) and the local (Martin *et al.*, 2007) crystal structures, and neutron powder diffraction has been combined with molecular dynamics to investigate thermal motions in the high-temperature cubic phase (Street *et al.*, 1997). The structural crystallography of the orthorhombic phase has been studied at low temperatures using powder neutron diffraction, at medium resolution, by Mitchell *et al.* (2007), and at significantly higher resolution by Knight (2014) who found negative linear thermal expansion for the *b* axis (*Pbnm* setting) between 20 K – 90 K, and evidence for quadratic coupling of the in-phase tilt to the anti-phase tilt. Of particular relevance to this current communication are the results and conclusions drawn by Zhao *et al.* (1993a,b) in two papers published in Physics of the Earth and Planetary Interiors, which for convenience in this article, we name PEPI I (Zhao *et al.*, 1993a), and PEPI II (Zhao *et al.*, 1993b).

PEPI I describes the evolution of the crystal structure of neighborite between 293 K and 1173 K using both laboratory and synchrotron source X-ray powder diffraction. The crystallographic results from this paper were subsequently used to infer the critical behaviour of the orthorhombic – cubic phase transition, as detailed in PEPI II. Despite the apparently comprehensive nature of this study, Knight (2014) has shown it to be substantially flawed, containing inconsistent crystallographic results, poorly determined order parameter magnitudes, incorrect application of Landau theory, and a mathematical error that leads to the wrong conclusion concerning the critical exponent associated with the phase transition.

In PEPI I, laboratory source data were only collected to a Q resolution of 5.23 $Å^{-1}$ which is insufficient to derive precise structural parameters from a pseudosymmetric crystal structure (see Knight *et al.* (2004) for discussion of an example of an incorrect space group and implausible crystal structure, at ambient temperature and pressure, for $KCaF_3$ perovskite derived from data collected to a similar resolution). The derived structural parameters (bond lengths and angles) shown in Table 3 of PEPI I are inconsistent with estimated standard deviations (esds) of the structural parameters listed in Table 2, and bond length corrections for thermal motion are based on a model that assumes uncorrelated atomic displacements, which is inappropriate for a 3-dimensional, fully-connected, polyhedral network-structure. The order parameters for zone-boundary tilted perovskite phases are proportional to the amplitudes of displacements that transform as the basis vectors of the irreducible representations (irreps) R_4^+ (anti-phase tilt, Glazer, 1972), and M_3^+ (in-phase tilt, Glazer, 1972) of the cubic Brillouin zone (Cowley, 1964). The expressions for the two tilts used in PEPI I are only approximations to these amplitudes, and are derived assuming that all octahedral distortive modes are absent, which will not be the case. The correct method of analysis of the

atomic displacements is given by a full mode decomposition of the crystal structure (Perez-Mato *et al.*, 2010), which in the case of a perovskite crystal structure (ABC_3) in space group *Pnma*, contains 2 mode amplitudes associated with the A site, and 5 associated with the anions bonded to the octahedral B site (Cochran and Zia, 1968; Knight 2009, 2011, 2014).

In PEPI II, the magnitudes of the tilt angles, as determined by the methods detailed in PEPI I, were used in a simplified Landau free energy expression to determine the critical behaviour associated with the orthorhombic – cubic phase transition. It was assumed, without justification, that quartic terms could be ignored, leading to the expressions below

$$\frac{\partial G}{\partial q_4} = 0 = A_1\left(T - T_{c1}\right)q_4 + C_1 q_4^5 + \lambda q_4 q_2^2$$
$$\frac{\partial G}{\partial q_2} = 0 = A_2\left(T - T_{c2}\right)q_2 + C_2 q_2^5 + \lambda q_4^2 q_2$$

where q_2 is the magnitude of the in-phase tilt, q_4 is the magnitude of the anti-phase tilt, A_1, A_2, C_1, C_2 are Landau coefficients, and λ is a coupling coefficient. These equations are *simultaneous*, *non-linear* and *coupled*, and hence only have closed solutions for particular values of the Landau and coupling coefficients. However, the solutions to q_2 and q_4 given in PEPI II have been derived from an assumption that these equations are *independent*, and based on this mathematical error, they have been found to have identical critical exponents of 0.25. This conclusion that the in-phase and anti-phase tilts exhibit simultaneous tricritical behaviour violates Landau theory for continuous phase transitions as the two order parameters have different symmetries (Tolédano and Tolédano, 1987), and hence the conclusions for critical behaviour in neighborite drawn in PEPI II are formally invalid.

Results

In the present study, the normalised neutron powder diffraction patterns were examined for the presence or absence of key superlattice reflections at the R, M, and X points of the pseudocubic Brillouin zone. By 999 K, all X point reflections were too weak for reliable characterisation and the analysis presented here is, therefore, based on the stronger R and M point superlattice peaks. It should be noted, however, that, since the X point is only a reciprocal lattice point in the orthorhombic phase by virtue of the *simultaneous* presence of the R and M points, its absence does not affect the conclusions drawn.

The temperature dependences of the two strongest groups of diagnostic superlattice reflections in the temperature interval 1031 K – 1050 K, indexed in the pseudocubic setting as 3/2 1/2 1 (M point, $d \sim 2.1$Å), and 3/2 3/2 1/2 (R point, $d \sim 1.8$Å), are shown in Figure 1. The disappearance of the R point reflection, which is associated with the anti-phase octahedral tilt, and cation and anion displacements that transform as the irreps R_4^+ and R_5^+ respectively (Cochran and Zia, 1968; Knight, 2009, 2011), can be seen to have occurred between 1046 K and 1047 K. At 1047 K, the M point superlattice reflection, which is associated with the in-phase tilt and anion displacements that transform as the irreps M_3^+ and M_2^+ respectively (Cochran and Zia, 1968; Knight, 2009, 2011), still has appreciable intensity, but can be seen from the Figure to vanish at a slightly higher temperature, in the interval 1048 K – 1049 K. Analysis of the full diffraction pattern measured at 1047 K shows the absence of all reflections associated with the R and X points of the pseudocubic Brillouin zone, whereas the diffraction pattern collected at 1049 K is consistent with the aristotype structure, and exhibits no superlattice reflections at all. From these results it is clear that the apparently continuous phase transition from *Pbnm* to $Pm\bar{3}m$ in fact proceeds by an intermediate phase that exists in the very small range of temperature between ~1046.5 K and ~1048.5 K. Of the

four space groups consistent with the perovskite structure and in-phase tilting alone, *i.e.* exhibiting superlattice reflections only at the M point of the pseudocubic Brillouin zone (Howard and Stokes, 1998), structural phase transitions from *Pbnm* to space groups *Immm*, *I*4/*mmm* and $Im\bar{3}$ are first order, with a second-order transition being permitted only to *P*4/*mbm* (Stokes and Hatch, 1988). Structural phase transitions to the aristotype phase are first order for the space groups *Immm* and *I*4/*mmm* as they violate the Landau condition, but permitted to be continuous for space groups $Im\bar{3}$ and *P*4/*mbm* (Stokes and Hatch, 1988). From these results, together with the observation of a lambda anomaly in the heat capacity which excludes the possibility of a first-order transition (Torpor at al., 1997), we conclude that the intermediate phase must be tetragonal, in space group *P*4/*mbm*. To test this conclusion, the data collected at 1047 K have been fitted using the Rietveld method. In this refinement, the starting value for the *x* coordinate of the fluorine anion on the Wyckoff site 4*g* was derived from the magnitude of the in-phase tilt determined from the crystal structure of the orthorhombic phase at 1044 K (Knight, 2009, 2011). Convergence from this starting point was rapid, with Figure 2 showing the excellent fit to the data, indicating the correctness of the model; on the same figure, we make comparisons with data analysed in the orthorhombic phase at 1033 K, and the cubic phase at 1049 K. Fractional coordinates, atomic displacement parameters, unit cell dimensions, and agreement factors for the three phases are reported in Table 1.

In Figure 3 we show the temperature evolution of the pseudocubic subcell in the orthorhombic phase, and the cubic lattice parameter above the second phase transition temperature. The pseudocubic subcell, subscripted *p*, is related to the orthorhombic unit cell via the transformation -1/2 1/2 0 / 1/2 1/2 0 / 0 0 1/2, and can be best described using the monoclinic metric $a_p = b_p \neq c_p$, $\alpha_p = \beta_p = 90°$, $\gamma_p \neq 90°$ since this description, with $\gamma_p \neq 90°$, most clearly reveals that the 4-fold rotation in the cubic phase is reduced to a 2-fold rotation

in the orthorhombic phase (Knight, 2011). The lattice parameters are continuous through the phase transition, and hence there is no volume discontinuity at the phase transition temperature, although there is a clear change in gradient of the linear thermal expansion coefficient. Critical exponents for structural phase transitions are generally determined from the temperature-dependence of superlattice reflections measured on single crystals. However, in the case of powder diffraction data where these weak reflections are more difficult to measure, the temperature variation of the spontaneous strain and internal coordinates is normally the method of choice (Carpenter, 2007). The cosine of the pseudocubic inter-axial angle γ_p is essentially identical to the spontaneous strain component e_6 (e_4 in the Cartesian basis of Carpenter, 2007) which varies as the square of the order parameter q_4, which in turn is related to the magnitude of the anti-phase tilt (Carpenter, 2007). The fit to the γ_p data in Figure 3 is based on simple critical behaviour $\left(90\text{-}\gamma_p\right) = \mathrm{A}\left(1-\mathrm{T}/\mathrm{T_c}\right)^{\beta}$ where A is a constant, T_c is the critical temperature, and β is a critical exponent. Within error, $\beta = 0.5$, and hence the critical exponent for the order parameter of the *Pbnm* to *P*4/*mbm* phase transition is 0.25, and the transition is tricritical in nature. Confirmation of the critical exponent can usually be achieved by determining the temperature-dependence of the order parameters directly from the fractional coordinates and the unit-cell parameters. In the case of perovskite-structured materials, as we have pointed out earlier, the order parameters should be determined through mode decomposition. Unfortunately, in the case of neighborite, the MgF_6 octahedron is subject to large amplitude librations at temperatures close to the first, and second phase transitions (Street *et al.*, 1997). As a result, since the refinement of the atomic displacement parameters are based on Gaussian probability density functions, the true location of the atomic positions, as determined from Bragg scattering, is severely compromised, with an apparent shortening of the Mg-F bonds being observed (Zhao *et al.*, 1993a, b). As a consequence of this, mode decomposition cannot be used to derive a reliable confirmatory

critical exponent. However, at temperatures below 440 K, where librational motion can be safely ignored, Knight (2014) has indeed found that the order parameter q_4 varies with critical exponent 0.25, and furthermore, that the order parameter q_2 is quadratically coupled to q_4. At low temperatures, the behaviour of neighborite is therefore dominated by the anti-phase tilt and the thermal evolution is such that only the R point behaves in a critical manner. Whether this behaviour extends to the *Pbnm* – *P*4/*mbm* phase transition will require a detailed single crystal study of the temperature-dependence of the superlattice reflection intensities; however, the temperature-dependence of e_6, which depends on q_4^2 in the numerator (McKnight *et al.*, 2009), strongly suggests that this is so. The unusual development of the other spontaneous strains at the gamma point around 700 K that has been discussed by Carpenter *et al.* (1998) may arise from changes in the coupling between q_2 and q_4 which are necessary for the evolution of the tetragonal phase, in which only q_2 is the active order parameter.

In the case of the first structural phase transition, the narrowness of the tetragonal phase field precludes further analysis of the data presented here and also explains the fact that the tetragonal phase of $NaMgF_3$ has not been reported previously. In each of the two X-ray diffraction experiments reported by Zhao *et al.* (1993a), data were collected isothermally but in steps that were too large (~20 K in the vicinity of the transitions) to resolve the two phase transitions, whereas, in the more recent study of the local structure of $NaMgF_3$ by Martin *et al.* (2007), data were collected as the sample temperature was increased continuously, so the diffraction pattern recorded at each datum was integrated over a 16 K range.

Implications for terrestrial mineralogy and geophysics

It might be argued that the subtleties of the ferroelastic phase transformations in perovskites are of limited relevance to our understanding of the Earth, as it is now generally accepted that the major perovskite phase, $MgSiO_3$, will remain orthorhombic throughout the lower mantle from its formation until the transition to the post-perovskite structure that occurs close to the core-mantle boundary (Murakami *et al.*, 2004; Oganov and Ono, 2004). This statement, however, is not true for $CaSiO_3$ perovskite, thought to be the third most abundant lower mantle mineral, and which also exists as a major component in subducted mid-ocean ridge basalt. Although $CaSiO_3$ may, or may not, be cubic under lower mantle conditions (see e.g. Noguchi *et al.*, 2013) it is definitely known to exhibit lower symmetry under conditions which many workers have considered to be geologically relevant. There is, however, currently no consensus as to the number of high-temperature phase transitions (one or two), the transition temperatures, or the space groups of the lower-symmetry phases of this mineral. At 40 GPa, for example, the transitions have been reported in a range from 550 K (e.g. Komabayashi *et al.*, 2007) to greater than 4000 K (Li *et al.*, 2006). Space groups suggested by computer simulation studies include *I*4*/mcm* and *Imma* (Adams and Oganov, 2006) or *Pbnm* and a tetragonal phase (Li *et al.*, 2006; probably *I*4*/mcm* or *P*4*/mbm* from the discussion in their paper). X-ray diffraction experiments by Uchida *et al.* (2009) gave data that they considered consistent with *Cmcm* or possibly *Pbnm*, whereas other workers have been more cautious and reported only that their diffraction patterns indicated a tetragonal crystal system (Komabayashi *et al.*, 2007). Understanding ferroelasticity in these systems is crucial to our understanding of the Earth. Not only will the phase transitions themselves cause potential seismic anomalies (see e.g. Komabayashi *et al.*, 2007, for discussion of this point with relevance to $CaSiO_3$), but also, even if a transition to a higher-symmetry structure does not occur, ferroelastic twinning induced by seismic waves may cause a large seismic

attenuation, as determined in a recent study by Li and Weidner (2012) once again using $NaMgF_3$ as an analogue for the silicate perovskites.

Acknowledgements

We are grateful for the careful reviews of this article by Prof M A Carpenter and an anonymous reviewer. This work was supported by the Natural Environment Research Council (ref. NE/J009520/1). IGW thanks J P Brodholt and D P Dobson for helpful discussions.

References

Adams DJ, Oganov AR (2006) Ab initio molecular dynamics study of $CaSiO_3$ perovskite at P-T conditions of Earth's lower mantle. Phys Rev B 73:184106

Carpenter MA (2007) Elastic anomalies accompanying phase transitions in $(Ca,Sr)TiO_3$ perovskites: Part I. Landau theory and a calibration for $SrTiO_3$. Am Mineral 92:309–327

Carpenter MA, Salje EKH, Graeme-Barber A (1998) Spontaneous strain as a determinant of thermodynamic properties for phase transitions in minerals. Eur J Mineral 10:619-691

Chen J, Liu H, Martin CD, Parise JB, Weidner DJ (2005) Crystal chemistry of $NaMgF_3$ perovskite at high pressure and temperature. Am Mineral 90:1534-1539

Chao ECT, Evans HT, Skinner BJ, Milton C (1961) Neighborite, $NaMgF_3$, a new mineral from the Green River Formation, South Ouray, Utah. Am Mineral 46: 379-393

Cochran W, Zia A (1968) Structure and dynamics of perovskite-type crystals. Phys Status Solidi 25:273–283

Cowley RA (1964) Lattice dynamics and phase transitions of strontium titanate. Phys Rev 134:A981–A997

Dobson DP, Hunt SA, Lindsay-Scott A, Wood IG (2011) Towards better analogues for $MgSiO_3$ post-perovskite: $NaCoF_3$ and $NaNiF_3$, two new recoverable fluoride post-perovskites. Phys Earth Planet Inter 189:171-175

Dobson DP, Miyajima N, Nestola F, Alvaro M, Casati N, Liebske C, Wood IG, Walker AM (2013) Strong inheritance of texture between perovskite and post-perovskite in the D″ layer. Nature Geoscience 6:575-578

339 Glazer AM (1972) The classification of tilted octahedra in perovskites. Acta Crystallogr B
340 28:3384–3392

341 Glazer AM (1975) Simple ways of determining perovskite structures. Acta Crystallogr A
342 31:756–762

343 Grocholski B, Shim S-H, Prakapenka V.B. (2010) Stability of the $MgSiO_3$ analog $NaMgF_3$
344 and its implication for mantle structure in super-Earths. Geophys Res Lett 37:L14204

345 Howard CJ, Stokes HT (1998) Group-theoretical analysis of octahedral tilting in perovskites.
346 Acta Crystallogr B 54:782–789

347 Hustoft J, Catalli K, Shim S-H, Kubo A, Prakapenka VB, Kunz M (2008) Equation of state of
348 $NaMgF_3$ postperovskite: Implications for the seismic velocity changes in the D″ region.
349 Geophys Res Lett 35:L10309

350 Ibberson R M, David WIF, Knight K S (1992) Report RAL-92-031. Rutherford Appleton
351 Laboratory, Didcot, Oxfordshire, England.

352 Knight KS (2009) Parameterization of the crystal structures of centrosymmetric zone-
353 boundary-tilted perovskites: An analysis in terms of symmetry-adapted basis-vectors of the
354 cubic aristotype phase. Can Mineral 47:381–400

355 Knight KS (2011) Centrosymmetric perovskite crystal structures with space group Pbnm:
356 Crystallographic parameterization of $KCaF_3$ between 100 and 400 K in terms of the
357 amplitudes of symmetry-adapted basis-vectors of the cubic aristotype phase. Can Mineral:
358 49:793–808

359 Knight KS (2014) A high resolution neutron diffraction study of the crystal structure of
360 neighborite ($NaMgF_3$) between 9 K and 440 K. Am Mineral 99:824-838

Knight KS, Darlington CNW, Wood IG (2004) The crystal structure of $KCaF_3$ at 4.2 and 300 K: A re-evaluation using high-resolution powder neutron diffraction. Powder Diffr 20:7–13

Komabayashi T, Hirose K, Sata N, Ohishi Y, Dubrovinsky LS (2007) Phase transition in $CaSiO_3$ perovskite. Earth Planet Sci Lett 260:564–569

Larson AC, Von Dreele RB (1986) GSAS, general structure analysis system. Los Alamos National Laboratory Report No. LAUR 86-748

Li L, Weidner DJ, Brodholt J, Alfè D, Price GD, Caracas R, Wentzcovitch R (2006) Phase stability of $CaSiO_3$ perovskite at high pressure and temperature: insights from ab initio molecular dynamics. Phys Earth Planet Inter 155:260–268

Li L, Weidner DJ (2012) Anelasticity and transient creep in $NaMgF_3$ perovskite at high pressure. Phys Earth Planet Inter 194-195:98–106

Liu H-Z, Chen J, Hu J, Martin CD, Weidner DJ, Häusermann D, Mao H-K (2005) Octahedral tilting evolution and phase transition in orthorhombic $NaMgF_3$ perovskite under pressure. Geophys Res Lett 32:L04304

Martin CD, Chaudhuri S, Grey CP, Parise JB (2005) Effect of A-site cation radius on ordering of BX_6 octahedra in (K,Na)MgF_3 perovskite. Am Mineral 90:1522-1533

Martin CD, Chupas PJ, Chapman KW, Parise JB (2007) Local versus average structure: a study of neighborite ($NaMgF_3$) utilizing the pair distribution function method for structure determination. J Appl Crystallogr 40:441-448

Martin CD, Crichton WA, Liu HZ, Prakapenka V, Chen JH, Parise JB (2006a) Phase transitions and compressibility of $NaMgF_3$ (Neighborite) in perovskite and post-perovskite-related structures. Geophys Res Lett 33:L11305

Martin CD, Crichton WA, Liu H, Prakapenka V, Chen J, Parise JB (2006b) Rietveld structure refinement of perovskite and post-perovskite phases of $NaMgF_3$ (Neighborite) at high pressures. Am Mineral 91: 1703–1706

McKnight REA, Howard CJ, Carpenter MA (2009) Elastic anomalies with transformation sequencies in perovskites: I. Strontium zirconate, SrZrO3. J Phys-Condens Mat 21:015901.

Mitchell RH, Alexander M, Cranswick LMD, Swainson IP (2007) A powder neutron diffraction study of the fluoroperovskite $NaMgF_3$ (neighborite) from 300 K to 3.6 K. Phys Chem Minerals 34:507–712

Murakami M, Hirose K, Kawamora K, Sata N, Ohishi Y (2004) Post perovskite phase transition in $MgSiO_3$. Science 304:855–858

Noguchi N, Komabayashi T, Hirose K, Ohishi Y (2013) High-temperature compression experiments of $CaSiO_3$ perovskite to lowermost mantle conditions and its thermal equation of state. Phys Chem Minerals 40:81-91

Oganov AR, Ono S (2004) Theoretical and experimental evidence for a post-perovskite phase of $MgSiO_3$ in Earth's D″ layer. Nature 430:445–448

Perez-Mato JM, Orobengoa D, Aroyo MI (2010) Mode crystallography of distorted structures. Acta Crystallogr A, 66:558-590

Poirier JP, Peyronneau J, Gesland JY, Brebec G (1983) Viscosity and conductivity of the lower mantle: an experimental study on a $MgSiO_3$ perovskite analogue, $KZnF_3$. Phys Earth Planet Inter 32:273-287

Stokes HT, Hatch DM (1988) Isotropy subgroups of the 230 crystallographic space groups. World Scientific Press, Singapore, 603 pp

405 Street JN, Wood IG, Knight KS, Price GD (1997) The influence of thermal vibrations on the
406 average structure of cubic $NaMgF_3$ perovskite: a combined molecular dynamics and neutron
407 diffraction study. J Phys Condens Matter 9:L647–L655

408 Tolédano J-C, Tolédano P (1987) The Landau theory of phase transitions. World Scientific
409 Press, Singapore, 451 p

410 Torpor L, Navrotsky A, Zhao Y, Weidner DJ (1997) Thermochemistry of fluoride
411 perovskites: Heat capacity, enthalpy of formation, and phase transition of $NaMgF_3$. J Solid
412 State Chem 132:131–138

413 Uchida T, Wang Y, Nishiyama N, Funakoshi K, Kaneko H, Nozawa A, Von Dreele RB,
414 Rivers ML, Sutton SR, Yamada A, Kunimoto T, Irifune T, Inoue T, Li B (2009) Non-cubic
415 symmetry of $CaSiO_3$ perovskite up to 18 GPa and 1600 K. Phys Earth Planet Inter: 282:268-
416 274

417 Umemoto K, Wentzcovitch RM (2006) Potential ultrahigh pressure polymorphs of ABX_3
418 compounds. Phys Rev B 74:224105

419 Umemoto K, Wentzcovitch RM, Weidner D J, Parise JB (2006) $NaMgF_3$: A low pressure
420 analog of $MgSiO_3$. Geophys Res Lett, 33:L15304

421 Watson GW, Wall A, Parker SC (1995) A molecular dynamics simulation of the effect of
422 high pressure on fast-ion conduction in a $MgSiO_3$-perovskite analogue; $KCaF_3$. Phys Earth
423 Planet Inter 89:137-144

424 Zhao Y, Weidner DJ, Parise JB, Cox DE (1993a) Thermal expansion and structural distortion
425 of perovskite – data for $NaMgF_3$ perovskite. Part I. Phys Earth Planet Inter 76:1–16

426 Zhao Y, Weidner DJ, Parise JB, Cox DE (1993b) Critical phenomena and phase transition of
427 perovskite - data for $NaMgF_3$ perovskite. Part II. Phys Earth Planet Inter 76: 17–34

Figure Captions

Figure 1

The temperature-dependence of representative pseudocubic superlattice reflections at the M and R points of the pseudocubic Brillouin zone of $NaMgF_3$. The R point reflection 3/2 3/2 1/2 (d ~ 1.8Å, orthorhombic reflections: 1 2 3 + 2 1 3 + 3 0 1) can be seen to vanish at a temperature just greater than 1046 K, whereas the M point reflection 3/2 1/2 1(d ~ 2.1Å, orthorhombic reflections: 1 2 2 + 2 1 2, tetragonal reflection 2 1 1) passes through this temperature and disappears between 1048 K and 1049 K. Consideration of group theoretical results and analysis of diffraction data shows the phase field composed of the M point superlattice reflections alone (~1046.5 K – 1048.5 K) corresponds to a new tetragonal polymorph of neighborite.

Figure 2

Rietveld fits to the three polymorphs of neighborite in the orthorhombic (*Pbnm*), tetragonal (*P*4/*mbm*) and cubic ($Pm\bar{3}m$) phases.

Figure 3

The temperature variation of the cubic and pseudocubic lattice parameters in the vicinity of the orthorhombic – tetragonal, tetragonal – cubic phase transitions. The full line on the figure shows that the pseudocubic shear angle varies with reduced temperature to the power 1/2, and hence the critical exponent for the tetragonal – orthorhombic phase transition is 1/4, i.e. tricritical in nature. The pseudocubic lattice parameters a_p, b_p and c_p are defined in terms of

those of the orthorhombic unit cell, *a*, *b* and *c* by: $a_p = b_p = \frac{\sqrt{a^2 + b^2}}{2}$, $c_p = c/2$ and

$$\cos\left(\gamma_p\right) = \frac{b^2 - a^2}{a^2 + b^2} \cong \frac{2\sqrt{2}a_0\left(b - a\right)}{4a_0^2} = \frac{\left(b - a\right)}{\sqrt{2}a_0} = e_6$$

where a_0 is the cell parameter of the cubic phase extrapolated into the tetragonal and orthorhombic phase fields.

454 Table 1. Crystallographic data for the three phases of $NaMgF_3$.

Structural parameters		*Pbnm* 1033 K	*P*4/*mbm* 1047 K	$Pm\bar{3}m$ 1049 K
Lattice Parameters (Å)	*a*	5.53822(3)	5.55376(4)	3.92695(1)
	b	5.55272(3)	*a*	*a*
	c	7.85132(4)	3.92846(5)	*a*
Unit cell volume ($Å^3$)		241.445(2)	121.170(1)	60.557(1)
Na	*x*	-0.0034(11)		
	y	0.5098(25)		
	$100u_{iso}(Å^2)$	7.45(10)	8.071(78)	8.107(75)
Mg	$100u_{iso}(Å^2)$	1.86(4)	2.560(48)	2.399(33)
F1	*x*	0.0439(6)		
	y	-0.0048(14)		
	$100u_{11}(Å^2)$	8.29(25)	11.46(56)	12.94(6)
	$100u_{22}(Å^2)$	7.99(34)	u_{11}	u_{11}
	$100u_{33}(Å^2)$	1.05(16)	0.84(26)	2.34(7)
	$100u_{12}(Å^2)$	0.24(33)		
	$100u_{eq}(Å^2)$	7(1)	7.9(3)	9.4(3)
F2	*x*	0.2836(4)	0.2612(5)	
	y	0.2169(4)		
	z	-0.0221(4)		
	$100u_{11}(Å^2)$	4.33(12)	8.52(35)	
	$100u_{22}(Å^2)$	4.31(13)	u_{11}	

$100u_{33}(Å^2)$	10.05(21)	13.18(52)
$100u_{12}(Å^2)$	-2.75(12)	-5.45(42)
$100u_{13}(Å^2)$	0.51(21)	
$100u_{23}(Å^2)$	-0.45(21)	
$100u_{eq}(Å^2)$	6.2(3)	10.1(7)

Pbnm. Na, F1: 4*c x, y,* 1/4; Mg: 4*a* 0, 0, 0; F2 8*d x, y, z* (Rp = 0.049, Rwp = 0.054, χ^2 = 1.6 for 30 variables)

*P*4/*mbm*. Na: 2*c* 0, 1/2, 1/2; Mg: 2*a* 0, 0, 0; F1: 2*b* 0, 0, 1/2; F2: 4*g x*, 1/2-*x*, 0 (Rp = 0.043, Rwp = 0.049, χ^2 = 1.3 for 19 variables)

$Pm\bar{3}m$. Na: 1*b* 1/2, 1/2, 1/2; Mg: 1*a* 0, 0, 0; F1: 3*d*, 0, 0, 1/2 (Rp = 0.043, Rwp = 0.049, χ^2 = 1.3 for 11 variables)

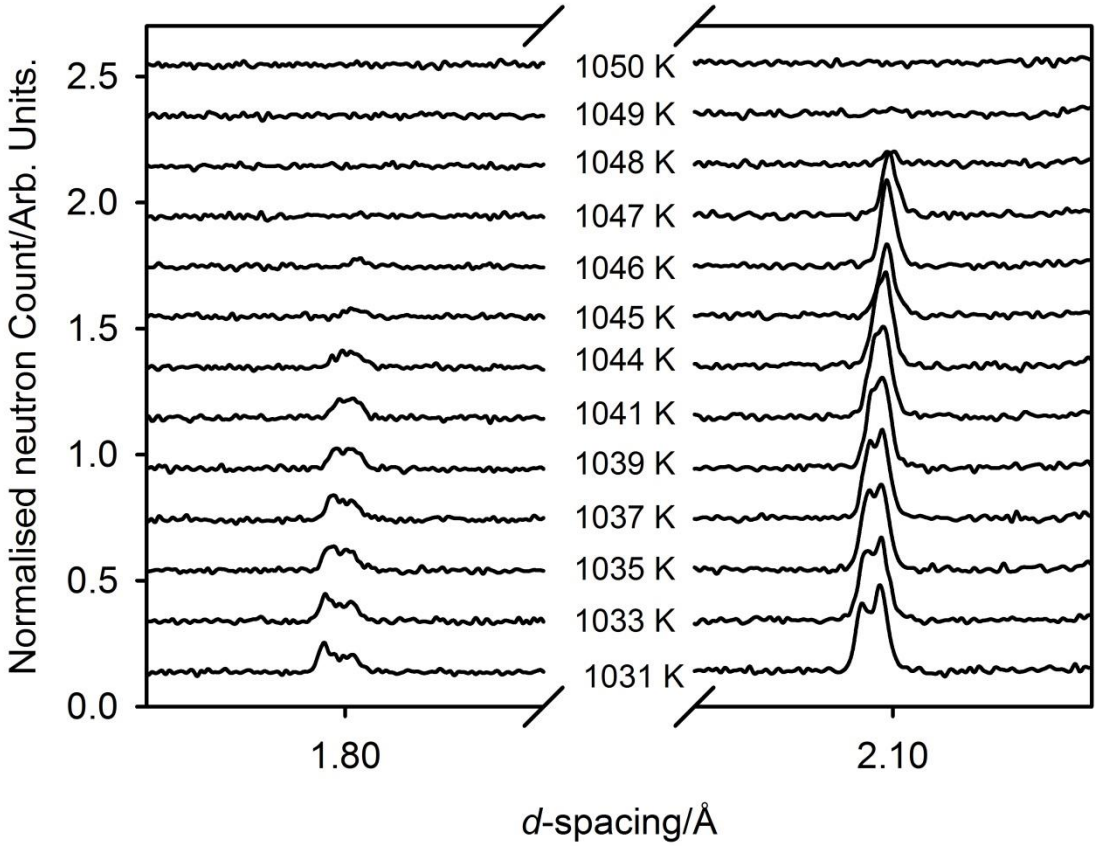

461

462 Figure 1.

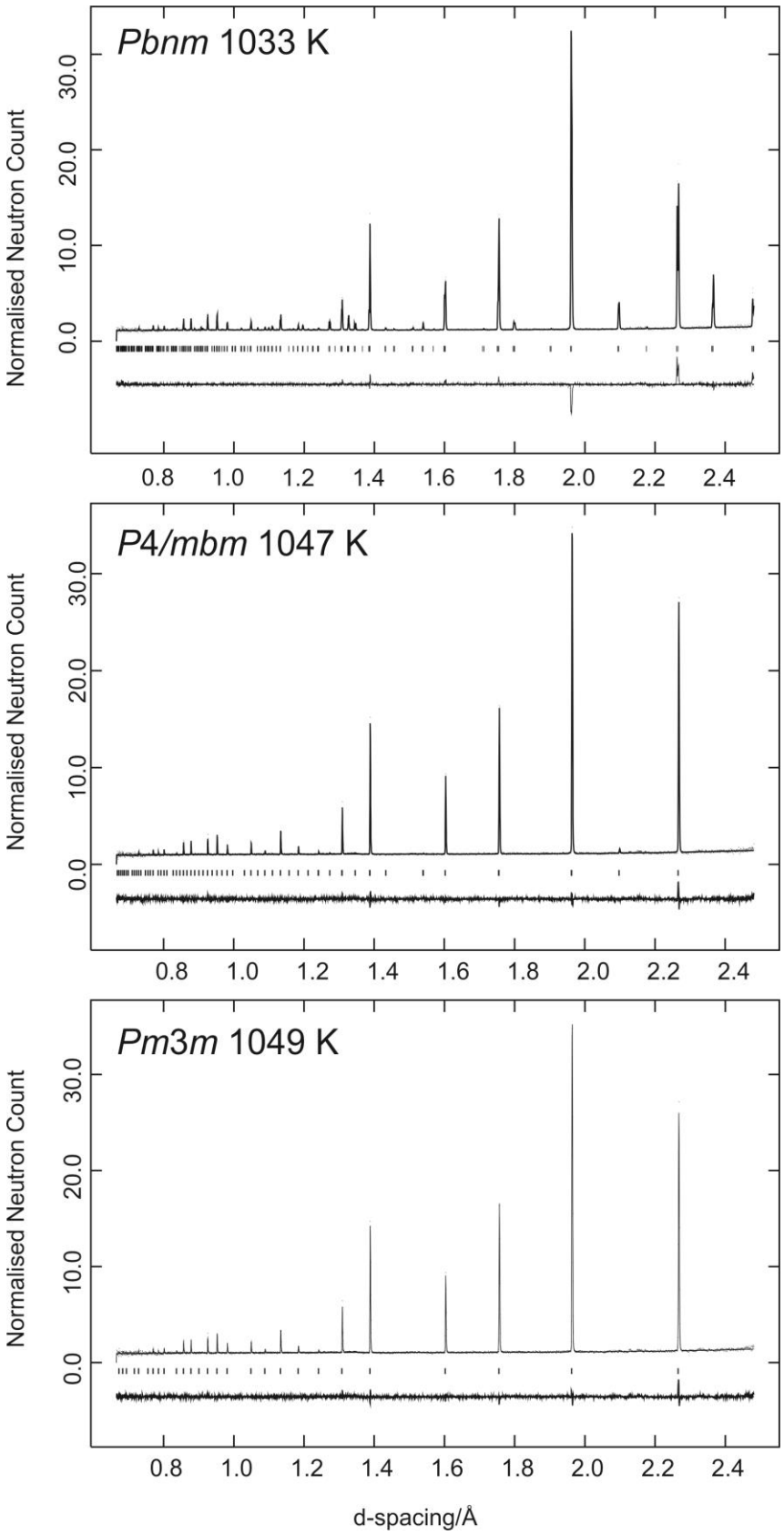

463

464 Figure 2.

465

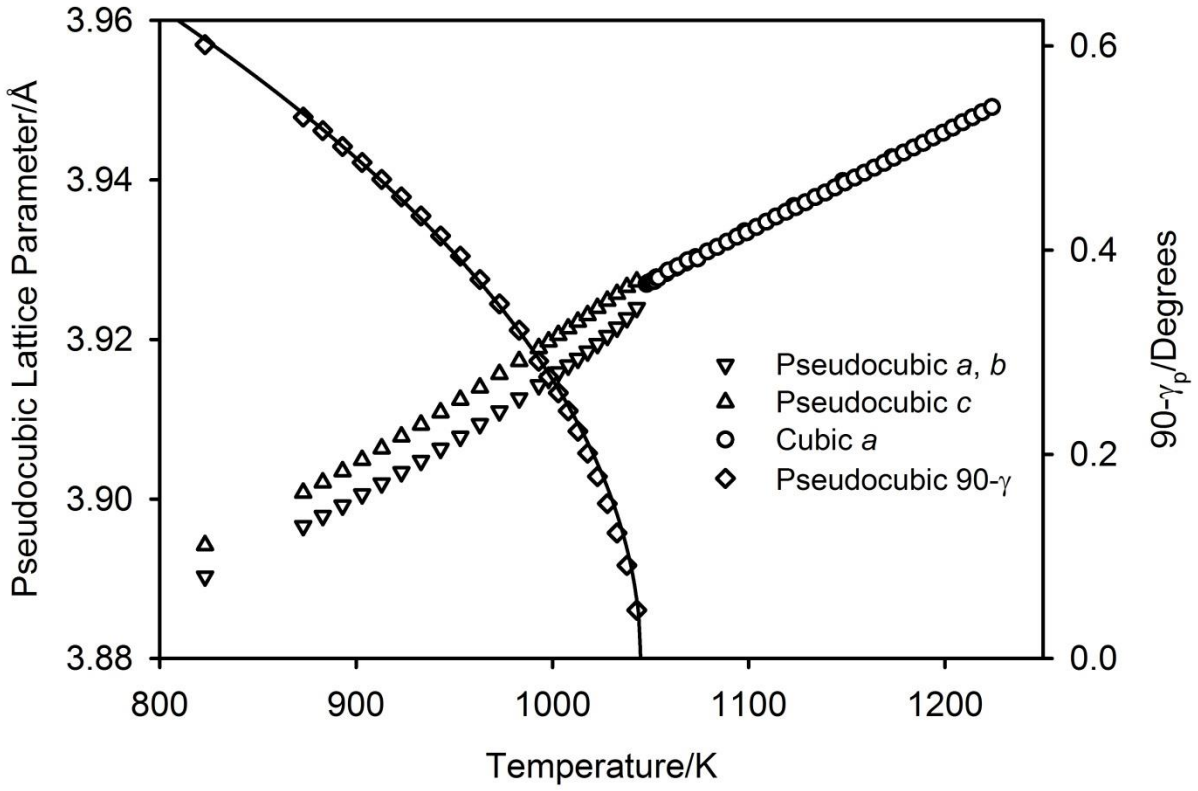

466

467 Figure 3.